

BCSJ Award Article

Unique Helical Triangle Molecular Geometry Induced by Dipole–Dipole Interactions

Takahito Ishikawa, Tomoyuki Morita, and Shunsaku Kimura*

Department of Material Chemistry, Graduate School of Engineering, Kyoto University, Kyoto-Daigaku-Katsura, Nishikyo-ku, Kyoto 615-8510

Received January 22, 2007; E-mail: shun@scl.kyoto-u.ac.jp

Novel helix-peptide wheels, in which three helices were connected by using a template, were prepared, and the dipole–dipole interactions among the helices were studied in relation to the formation of a planar triangle structure containing three helices. The helical segments had a 3_{10}-helix structure. ^{13}C spin-lattice relaxation time (T_1) measurements showed that the helical segments had restricted mobility. Deuterium exchange rates of amide protons were accelerated in the helix-peptide wheels compared to the respective linear helix peptides, suggesting that there is torsion on the cylindrical shape. Therefore, the predominant structure of the helix-peptide wheels is a planar triangle in solution. Further, the triangle structure was successfully transferred onto a gold substrate.

Nano-science using organic molecules has attracted much attention in various fields. One key factor for the development of nano-science is to prepare organic molecules with well-determined geometry in terms of regio- and stereo-specificity, configuration, and conformation. Recently, a trend to use larger molecules has become prominent in the field of materials science with the aim to produce high-performance and highly functional materials. However, it becomes difficult to control the structure of larger molecules. Advancements in covalent chemistry contribute greatly to the preparation of well-specified large molecules, but secondary interactions, such as hydrogen bonds,[1] electrostatic interaction,[2] and CH–π interaction,[3] etc., are also helpful to regulate the molecular shape. In the present study, another secondary interaction, dipole–dipole interaction, was examined for geometry regulation of three helices in one molecule.

Proteins are typical examples for molecular architecture with a highly regulated structure. In nature, helix bundles are a common motif in proteins, and exhibit a variety of physiological activities, such as acting as ion channels. On the other hand, a helix triangle, in which three peptide helices were connected in a cyclic way by covalent bonds to generate a planar structure, was prepared as an unprecedented helix assembly.[4] Interestingly, the cyclization yield of the linear three peptide helices connected in a series was relatively high, suggesting that the dipole–dipole interaction may promote the cyclization probability via an attractive electrostatic force between the *N*-terminal with a partial positive charge and the *C*-terminal with a partial negative charge of the linear precursor peptide. We, therefore, designed a new helix triangle without covalent bonds between the *N*-terminal and the *C*-terminal but with dipole–dipole interaction acting between them.

The molecular structures of the helix-peptide wheel, in which three helical peptides were connected by using the template molecule 1,3,5-benzenetricarboxylic acid through amide-bond formation with the side chains of the Lys residues located in the middle of the helical peptide chains, are shown in Fig. 1. The three helices either nonapeptide or hexapeptide can rotate freely around the linker bond to the template without steric collision due to the long length of the linker. The conformation of the helix-peptide wheel in solution and in monolayer on a gold substrate was studied by various spectroscopic methods to obtain information on the dipole–dipole interactions in terms of regulation of the molecular shape.

Experimental

Synthesis of Helical Peptides. Mono6, tri6, mono9, and tri9 were synthesized according to Scheme 1. All peptides were synthesized by the conventional liquid-phase method. All intermediates were identified by ^1H NMR spectroscopy, and some of them were further confirmed by fast atom bombardment (FAB) mass spectrometry. Final compounds were identified by ^1H NMR, ^{13}C NMR, FAB mass spectrometry, and matrix-assisted laser desorption/ionization time-of-flight (MALDI-TOF) mass spectrometry. The purity of each compound was checked by thin-layer chromatography (TLC). The solvent systems for TLC analysis were (A) chloroform/methanol (5/1 v/v), (B) chloroform/methanol (10/1 v/v), and (C) chloroform/methanol/ammonia water (13/5/1 v/v/v). Characterization of the precursors and final peptides was shown below with synthetic procedures for tri6 and tri9.

BA2KZA3M (mono6): TLC: R_f(A) = 0.63, R_f(B) = 0.50, R_f(C) = 0.86. ^1H NMR (400 MHz, CD_3CN): δ 1.27–1.46 (37H,

Published on the web August 10, 2007; doi:10.1246/bcsj.80.1483

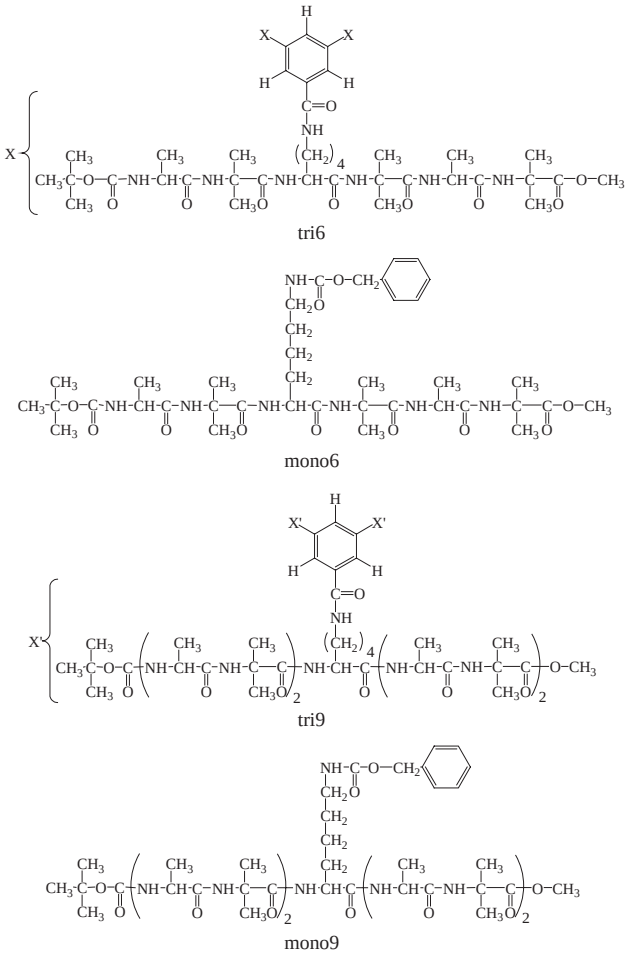

Fig. 1. Chemical structures of tri6, mono6, tri9, and mono9.

$(CH_3)_3CO$, AlaC$^{\beta}H$, AibCH_3, LysC$^{\gamma}H$, LysC$^{\delta}H$), 1.76 (2H, LysC$^{\beta}H$), 3.07 (2H, LysC$^{\varepsilon}H$), 3.59 (3H, OCH_3), 3.84 (1H, AlaC$^{\alpha}H$), 3.89 (1H, LysC$^{\alpha}H$), 4.09 (1H, AlaC$^{\alpha}H$), 5.03 (2H, $OCH_2C_6H_5$), 5.63 (1H, Lys$(CH_2)_4$NH), 5.93 (1H, urethaneNH), 7.24–7.36 (8H, AlaNH, AibNH, $OCH_2C_6H_5$), 7.45 (1H, LysNH), 7.59 (1H, AibNH). ^{13}C NMR (100 MHz, CD_3CN): a part of the spectrum is shown in Fig. 6. MS (FAB, matrix; (3-nitrophenyl)-methanol): m/z 792.5 (calcd for $C_{38}H_{62}N_7O_{11}$ $[(M+H)^+]$ m/z 792.4).

tri6: BA2KZA3M (2.02 g, 2.55 mmol) was dissolved in methanol, and 30 wt % Pd/C (610 mg) was added to the solution. The mixture was stirred at room temperature for 40 h under H_2 atmosphere. Pd/C was removed by filtration, and the solvent was removed by evaporation. The residue was washed with diisopropyl ether to afford BA2KA3M (1.44 g, 2.19 mmol). 1,3,5-Benzenetricarboxylic acid (triOH) (79.4 mg, 0.378 mmol) and BA2KA3M (1.44 g, 2.19 mmol) were dissolved in DMF, and HATU (851 mg, 2.24 mmol) and DIEA (572 µL, 3.28 mmol) were added to the solution at 0 °C. The solution was stirred at 0 °C for 30 min and thereafter at room temperature for 18 h under N_2 atmosphere. HATU (862 mg, 2.27 mmol) and DIEA (594 µL, 3.41 mmol) were added further to the solution, and the solution was stirred at room temperature for 24 h under N_2 atmosphere. Then, the solvent was removed by evaporation, and the residue was dissolved in ethyl acetate. The organic solution was washed with a saturated NaCl aqueous solution. The organic phase was dried and evaporated, and the residue was purified by using a Sephadex LH20 column with methanol as the eluent to afford a pure product (189 mg, 0.089 mmol, 24% yield). TLC: R_f(A) = 0.53, R_f(B) = 0.22, R_f(C) = 0.79. ^{1}H NMR (400 MHz, CD_3CN): δ 1.24–1.42 (105H, $(CH_3)_3CO$, AlaC$^{\beta}H$, AibCH_3, LysC$^{\gamma}H$), 1.60 (6H, LysC$^{\delta}H$), 1.80 (6H, LysC$^{\beta}H$), 3.38 (6H, LysC$^{\varepsilon}H$), 3.58 (9H, OCH_3), 3.80 (3H, AlaC$^{\alpha}H$), 3.90 (3H, LysC$^{\alpha}H$), 4.08 (3H, AlaC$^{\alpha}H$), 5.92 (3H, urethaneNH), 7.25 (3H, AlaNH), 7.33 (9H, Lys$(CH_2)_4$NH, AibNH), 7.49 (3H, LysNH), 7.59 (3H, AibNH), 8.34 (3H, aromatic). ^{13}C NMR (100 MHz, CD_3CN): a part of the spectrum is shown in Fig. 6. MS (FAB, matrix; (3-nitrophenyl)methanol): m/z 2129.3 (calcd for $C_{99}H_{166}N_{21}O_{30}$ $[(M+H)^+]$ m/z 2129.2). MS (MALDI-TOF, matrix; dithranol): m/z 2128.8 (calcd for $C_{99}H_{166}N_{21}O_{30}$ $[(M+H)^+]$ m/z 2129.2).

BA4KZA4M (mono9): TLC: R_f(A) = 0.67, R_f(B) = 0.47, R_f(C) = 0.85. ^{1}H NMR (400 MHz, CD_3CN): δ 1.28–1.45 (49H, $(CH_3)_3CO$, AlaC$^{\beta}H$, AibCH_3, LysC$^{\gamma}H$, LysC$^{\delta}H$), 1.80 (2H, LysC$^{\beta}H$), 3.06 (2H, LysC$^{\varepsilon}H$), 3.59 (3H, OCH_3), 3.84–4.09 (5H, AlaC$^{\alpha}H$, LysC$^{\alpha}H$), 5.01 (2H, $OCH_2C_6H_5$), 5.63 (1H, Lys$(CH_2)_4$-NH), 5.97 (1H, urethaneNH), 7.05 (1H, AlaNH), 7.29–7.37 (8H, AibNH, $OCH_2C_6H_5$), 7.43 (1H, LysNH), 7.57, 7.64, 7.72 (3H, AlaNH, AibNH). ^{13}C NMR (100 MHz, CD_3CN): a part of the spectrum is shown in Fig. 6. MS (FAB, matrix; (3-nitrophenyl)-methanol): m/z 1019.6 (calcd for $C_{48}H_{79}N_{10}O_{14}$ $[(M+H)^+]$ m/z 1019.6).

tri9: BA4KZA4M (610 mg, 0.599 mmol) was dissolved in methanol, and 20 wt % Pd/C (120 mg) was added to the solution. The solution was stirred at room temperature for 50 h under H_2 atmosphere. Pd/C was removed by filtration, and the solvent was removed by evaporation. The residue was washed with diisopropyl ether to afford BA4KA4M. TriOH (14.6 mg, 0.0695 mmol) and BA4KA4M were dissolved in DMF, and HATU (153 mg, 0.402 mmol) and DIEA (104 µL, 0.597 mmol) were added to the solution at 0 °C, and the solution was stirred at 0 °C for 30 min and thereafter at room temperature for 14 h under N_2 atmosphere. More HATU (152 mg, 0.400 mmol) and DIEA (104 µL, 0.597 mmol) were added to the solution, and the solution was stirred at room temperature for 29 h under N_2 atmosphere. The solvent was removed by evaporation, and the residue was purified by using a Sephadex LH20 column with methanol as the eluent to afford a pure product (100 mg, 0.0356 mmol, 51% yield). TLC: R_f(A) = 0.69, R_f(B) = 0.41, R_f(C) = 0.86. ^{1}H NMR (400 MHz, CD_3CN): δ 1.26–1.45 (141H, $(CH_3)_3CO$, AlaC$^{\beta}H$, AibCH_3, LysC$^{\gamma}H$), 1.58 (6H, LysC$^{\delta}H$), 1.84 (6H, LysC$^{\beta}H$), 3.34 (6H, LysC$^{\varepsilon}H$), 3.58 (9H, OCH_3), 3.82 (3H, AlaC$^{\alpha}H$), 3.92–3.96 (9H, AlaC$^{\alpha}H$, LysC$^{\alpha}H$), 4.07 (3H, AlaC$^{\alpha}H$), 6.05 (3H, urethaneNH), 7.06 (3H, AlaNH), 7.29 (3H, Lys$(CH_2)_4$NH), 7.35, 7.37, 7.39 (9H, AibNH), 7.46 (3H, LysNH), 7.56 (3H, AlaNH), 7.63 (3H, AibNH), 7.72 (3H, AlaNH), 8.27 (3H, aromatic). ^{13}C NMR (100 MHz, CD_3CN): a part of the spectrum is shown in Fig. 6. MS (FAB, matrix; (3-nitrophenyl)methanol): m/z 2810.5 (calcd for $C_{129}H_{217}N_{30}O_{39}$ $[(M+H)^+]$ m/z 2810.6). MS (MALDI-TOF, matrix; dithranol): m/z 2833.1 (calcd for $C_{129}H_{217}N_{30}O_{39}$ $[(M+H)^+]$ m/z 2832.6).

CD Spectroscopy. The CD spectra were measured in ethanol on a JASCO J-600 CD spectropolarimeter. The measurement was carried out in a quartz cell with a 0.1 cm optical pathlength. The residue concentration was in the range from 7.4×10^{-4} to 2.4×10^{-3} M (1 M = 1 mol dm^{-3}).

NMR Spectroscopy. The NMR measurements were performed on a Bruker DPX-400 NMR spectrometer (400 MHz). The sample temperature was 298 K. Samples were dissolved in CD_3CN. The relaxation times were measured under ^{1}H broadband

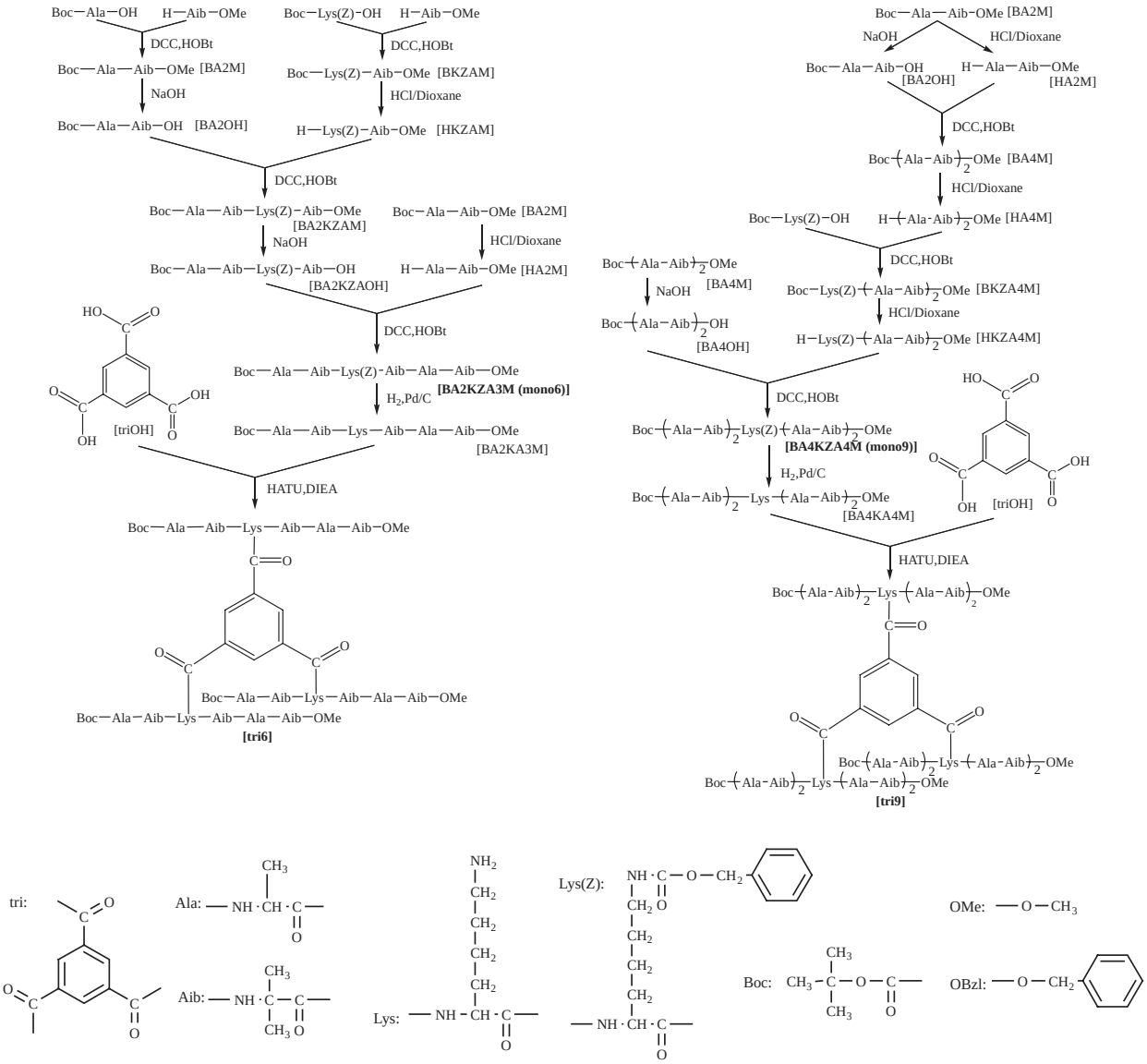

HATU:*o*-(7-azabenzotriazol-1-yl)-1,1,3,3-tetramethyluronium hexafluorophosphate
DIEA:*N*,*N*-diisopropylethylamine
DCC:1,3-dicyclohexylcarbodiimide
HOBt:1-hydroxybenzotriazole

Scheme 1. Synthetic scheme of mono6, tri6, mono9, and tri9.

decoupling using an inversion-recovery pulse sequence. The relaxation delay time was set as long as about 5 times the longest relaxation time of ^{13}C with protons, and 8 different intervals (t) between the 90 and 180° pulses were used in each experiment. The spin-lattice relaxation times were calculated by performing a three-parameter fit of the signal amplitudes I to the relaxation function $I = I_o[1 - A\exp(-t/T_1)]$ with the parameters I_o, A, and T_1.[5] The NMR tubes were sealed under inert gas.

Computational Geometry Optimization. The initial geometries of tri6 and tri9 were generated by using a Fujitsu CAChe WorkSystem 6.1.1 software.[6] For geometries with 3_{10}-helices, the dihedral angles of the peptide backbone were set to $\omega = 180°$, $\phi = -60°$, and $\psi = -30°$, respectively.[7] Each initial geometry was optimized by using the semiempirical Austin Model 1 (AM1) method in the MOPAC 2002 package.

Preparation of Monolayers at the Air/Water Interface and on Substrates. Preparation of the monolayers of tri6 and tri9 at the air/water interface and the transfer of the monolayers onto solid substrates were performed using a USI FSD-200A Langmuir trough at room temperature. Water purified by using a Millipore Milli-Q labo system (resistivity > 18 MΩ cm^{-1}) was used as water subphase. Tri6 and tri9 were dissolved in chloroform at concentrations of 7.0×10^{-4} and 7.4×10^{-4} M, respectively. The solution was spread on the water surface by using a microsyringe, and the monolayer was allowed to equilibrate for 15 min before compression. The π–A isotherms were recorded at a constant compression rate of 5–10 cm^2 min^{-1}. The monolayers on gold substrates were prepared by transferring the monolayer at the air/water interface onto the substrate at surface pressures of 15 and 20 mN m^{-1} (tri6 and tri9, respectively) by a vertical dipping method at upstroke. A gold substrate was used as a substrate for ellipsometry and infrared reflection–absorption spectroscopy (IRRAS). The size of a substrate is 13 mm × 76 mm with a 1 mm thickness. The gold substrate was prepared by vapor deposition

of chromium (300 Å) and thereafter 99.99% gold (2000 Å) onto a glass substrate that was cleaned with sulfonic acid prior to the metal deposition. The substrate was initially sunk into water prior to spreading the solution, and it was lifted up at a speed of 3 mm min^{-1} after compression of the monolayer.

Ellipsometry. The thicknesses of the tri6 monolayer and the tri9 monolayer on gold were determined on a MIZOJIRI DHA-OLX/S auto-ellipsometer at room temperature. A helium-neon laser of 632.8 nm was used as the incident light, and the incident angle was set at 70°. The thickness of the monolayer was calculated automatically by using the equipped program. In the calculation, the complex optical constant of the monolayer was assumed to be $1.50 + 0.00i$. The thickness was obtained as an average of more than 5 different spots on the monolayer.

IRRAS Measurements. IRRAS spectra of the tri6 monolayer and the tri9 monolayer on gold were recorded on a Nicolet Magna

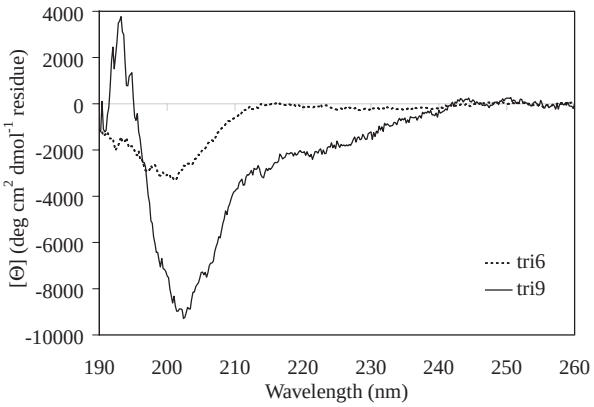

Fig. 2. CD spectra of tri6 and tri9 in ethanol at room temperature.

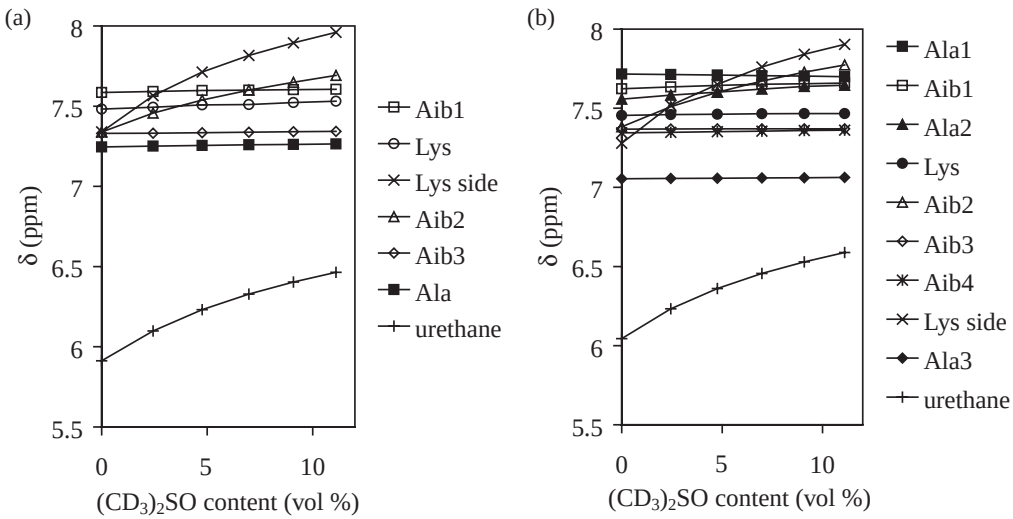

Fig. 3. Chemical shift changes of NH protons of (a) tri6 and (b) tri9 in CD_3CN with the addition of $(CD_3)_2SO$.

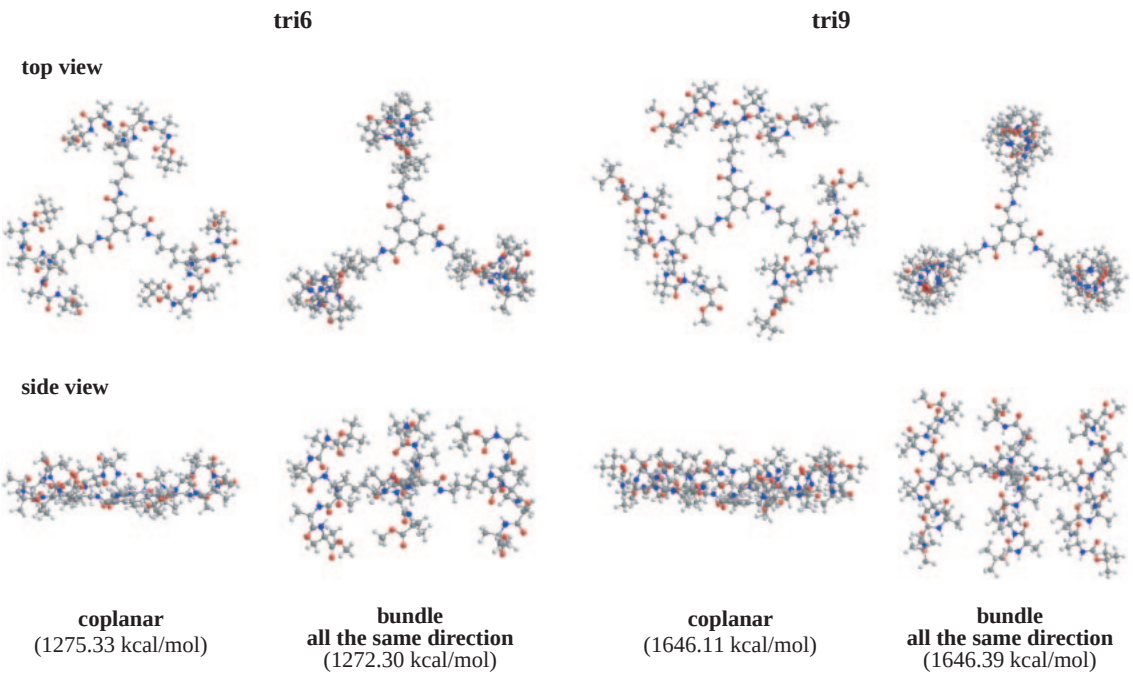

Fig. 4. Optimized geometries of tri6 and tri9 calculated by the AM1 method.

850 Fourier transform infrared spectrometer with a Harrick RMA-1DG/VRA reflection attachment at room temperature. The incident light was not polarized, and its incident angle was set at 85° from the surface normal. The number of interferogram accumulations was 200. The molecular orientation of the helical peptide unit in the monolayer was determined on the basis of the amide I/amide II absorbance ratio in the IRRAS spectrum according to Eq. 1 under the assumption that the helix axis was uniformly oriented around the surface normal.[8]

$$I_1/I_2 = 1.5((3\cos^2\gamma - 1)(3\cos^2\theta_1 - 1) + 2) / ((3\cos^2\gamma - 1)(3\cos^2\theta_2 - 1) + 2), \quad (1)$$

where I_i, γ, and θ_i ($i = 1$ or 2 corresponding to amide I or amide II) represent the observed absorbance, the tilt angle of helical axis from the surface normal, and the angle between the transition moment and the helix axis, respectively. The values of the θ_1 and θ_2 were taken to be 39 and 83°, respectively, considering 3_{10}-helical conformation.[9] All the measurements were performed at room temperature.

Results and Discussion

Conformation of Helical Segments. To investigate the peptide conformation of tri6 and tri9 in solution, CD spectroscopy was performed in ethanol. The CD spectra of the peptides are shown in Fig. 2. The spectrum of tri9 showed a sharp negative Cotton effect at around 203 nm and a broad shoulder at around 224 nm, which is typical for right-handed 3_{10}-helical conformation.[10] The spectrum of tri6 showed a negative Cotton effect at around 201 nm, but the peak intensity was weak. Therefore, tri6 should have a partial 3_{10}-helical conformation. These observations show that helix content of tri9 is higher than that of tri6.

To gain information on hydrogen bonds in the peptides, ^{1}H NMR spectroscopy was performed in a $(CD_3)_2SO/CD_3CN$ mixed solvent with different solvent ratios. The results are shown in Fig. 3. Chemical shifts of NH protons are plotted against the amounts of $(CD_3)_2SO$. In both peptides, chemical shifts of two amide protons in addition to the amide proton of Lys side chain shifted significantly to lower magnetic field with the addition of $(CD_3)_2SO$, which acts as a hydrogen acceptor. These results indicate that two main chain NH protons should be exposed to solvent, indicating that both peptides should take 3_{10}-helical conformation in acetonitrile, because two amide protons of two residues from the *N*-terminal are free from hydrogen bonds in 3_{10}-helical conformation.[9,11,12] This observation agrees with the result of CD spectroscopy.

In ^{1}H NMR spectra of tri6 and tri9, each proton of the peptides showed one peak, and the aromatic proton signal appeared as a singlet. Therefore, both peptides have C_3 symmetry on the NMR timescale.

Geometry Optimization. To obtain the plausible molecular structures of tri6 and tri9, geometry optimization was car-

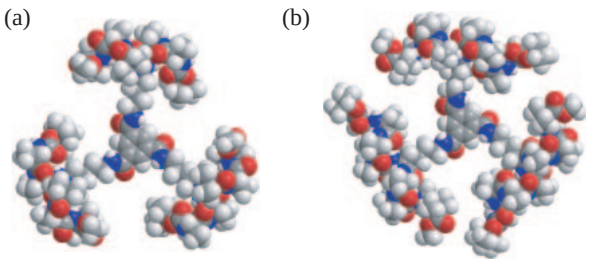

Fig. 5. Optimized geometries of (a) tri6 and (b) tri9 in a CPK model.

Table 1. NT_1 (s) of the Carbon Atoms in tri6, mono6, tri9, and mono9 in CD_3CN at 298 K[a)]

	tri6 MW: 2129.5	mono6 MW: 791.9	tri9 MW: 2811.3	mono9 MW: 1019.2
1. Ala(N-l) C^α	0.38	0.71	0.35	0.54
2. Ala(N-2) C^α			0.34	0.45
3. Lys C^α	0.41	0.60	0.32	0.38
4. Ala(C-l) C^α	0.34	0.69	0.27	0.36
5. Ala(C-2) C^α			0.32	0.47
6. Ala C^β	1.65 1.35	2.16 1.74	1.53 1.14 1.23	1.74 0.93 1.20 1.53
7. Lys C^β	0.40	1.10	0.30	0.36
8. Lys C^γ	0.52	1.00	0.50	0.72
9. Lys C^δ	0.36	1.14	0.32	0.72
10. Lys C^ε	0.44	1.18	0.52	0.80
11. Boc CH_3	1.78	2.52	1.59	2.04
12. OCH_3	4.50	7.20	3.87	5.25

a) *N* represents the number of protons attached to the carbon.

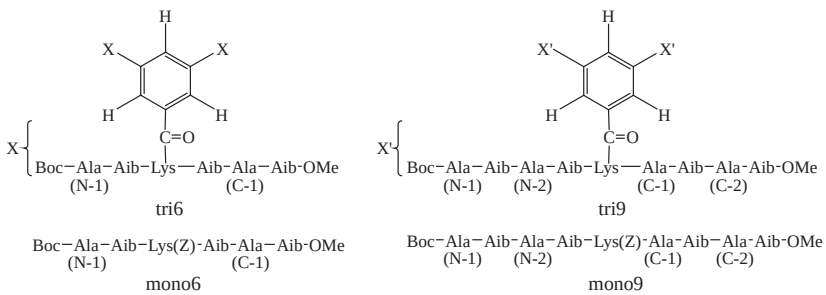

ried out by using the semi-empirical Austin Model 1 (AM1). According to the CD spectroscopy, the typical dihedral angles of a 3_{10}-helix ($\omega = 180^\circ$, $\phi = -60^\circ$, and $\psi = -30^\circ$)[7] were used for the backbone of the helical peptide units. Further, on the basis of the ^{1}H NMR spectroscopy, both peptides were considered to be C_3 symmetric. Two structures were built as initial geometries: a coplanar structure, in which the helix axes of three helical peptides were in the same plane, and a bundle structure, in which three helical peptides were all in the same direction. The geometry optimization led both peptides to take two stable structures, the coplanar structure where helix axes and the aromatic ring are in the same plane and the bundle structure where three helical peptides are all in the same direction with helix axes being perpendicular to the aromatic ring (Fig. 4). From two optimized geometries of the coplanar structures of tri6 and tri9 using a Corey–Pauling–Koltun (CPK) model, the peptide terminals of tri9 were close to each other (Fig. 5). It is therefore expected that dipole–dipole interactions among the helices is stronger in tri9 than in tri6 to promote the planar triangle structure of three helices in plane especially in tri9.

Mobility of Helical Segments by T_1 Measurements. To investigate the rotation mobility of the helical segments, ^{13}C spin-lattice relaxation times (T_1) of the helix-peptide wheels (tri6 and tri9) and the respective linear helix peptides (mono6 and mono9) were measured in CD_3CN at 298 K. Table 1 shows NT_1 of these peptides, where N represents the number of protons bound to the carbon. The ^{13}C NMR spectra of these peptides in CD_3CN are shown in Fig. 6. Generally, it is known that the shorter the correlation time is the longer the T_1 value becomes, because the mobility of carbon atom becomes higher. Therefore, the mobility of a helix segment in the wheel can be discussed on the basis of T_1.[13] T_1 values of C^α of Ala and Lys, which are involved in the backbone of the helix, were compared. In mono9, which is a linear nonapeptide, T_1 values of C^α showed a tendency to increase from the central residue of the helical segment, Lys, to the terminal residue, Ala. This observation can be reasonably explained by the fact that the helical terminals are more mobile than the helical center because of winding and unwinding motion of the terminals. In contrast, in the case of tri9, all T_1 values of C^α of Lys and Ala residues were comparable, suggesting that the terminal motions are suppressed in the wheel. Another explanation is that the linear nonapeptide, mono9, may rotate freely in solution to show longer T_1 values at the terminals, but in the case of tri9, the helix rotation is suppressed to show similar T_1 values all through the helix. The same feature was observed in the T_1 values for tri6 and mono6, but there was no remarkable trend. The intramolecular dipole–dipole interaction should be the reason for the mobility suppression of the helices in the helix-peptide wheels, and the predominant structure of the helix-peptide wheels should be a planar triangle in solution.

Solvent-Exposed Amide Protons by Deuterium Exchange Measurement. The mobility of helices in the helix-peptide wheels was further examined by measuring deuterium exchange rates of amide protons in tri9, mono9, tri6, and mono6. Deuterium exchange measurement generally provides both site-specific and quantitative information of the helix content.[14] To initiate the deuterium exchange reaction, 10 μL of

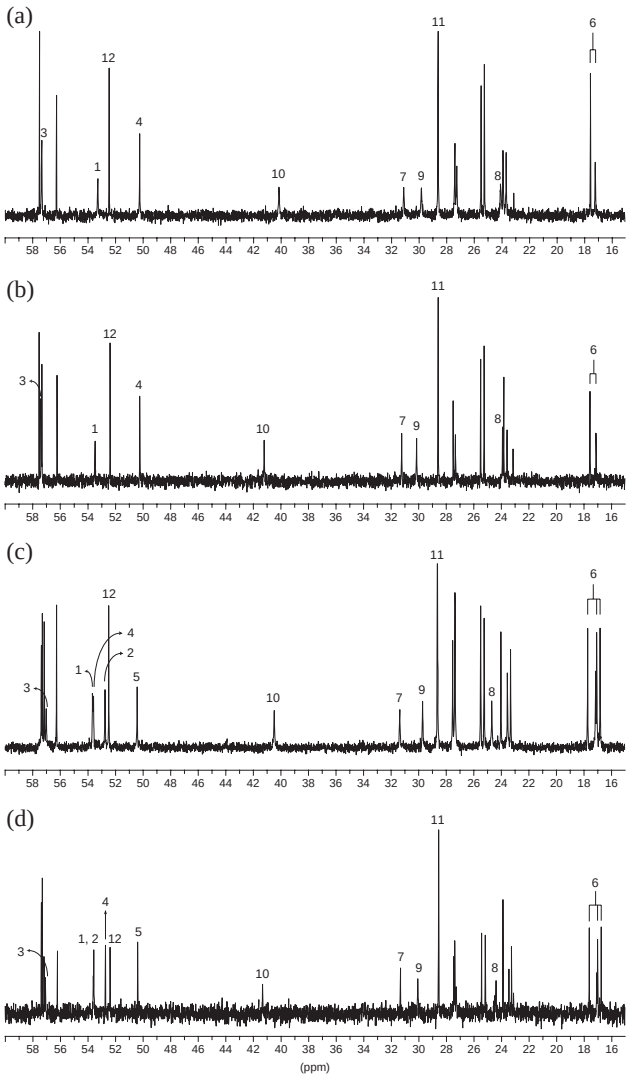

Fig. 6. ^{13}C NMR spectra of (a) tri6, (b) mono6, (c) tri9, and (d) mono9 in CD_3CN. Some of the carbons are numbered according to Table 1.

deuterated methanol was added to the solutions of tri9 and mono9 (both concentrations were 1.2 mg/500 μL), and 2 μL of deuterated methanol was added to the solutions of tri6 and mono6 (the concentrations were 0.8 mg/500 μL and 0.9 mg/500 μL, respectively). By comparing the spectra of tri9 and mono9, it was found that the exchange rates of Aib4 and Ala3 residues were faster in tri9 than those in mono9 within a given time (Figs. 7a and 7b). Similarly, the exchange rate of urethane residue in tri9 was faster than that in mono9. These observations apparently contradict the previous explanation for the mobility suppression of the helices in the wheel, because the low mobility may reduce the possibility of encounters between the amide proton and deuterated methanol by a dynamic process, thus slowing down the amide-proton exchange rate. However, there is another way to interpret the fast exchange rate in tri9, which is compatible with the suppressed mobility of the helices; the urethane group, Aib4, and Ala3 residues, which are located at the terminal end of the helix, should be distorted by the attractive force acting between the *N*-termi-

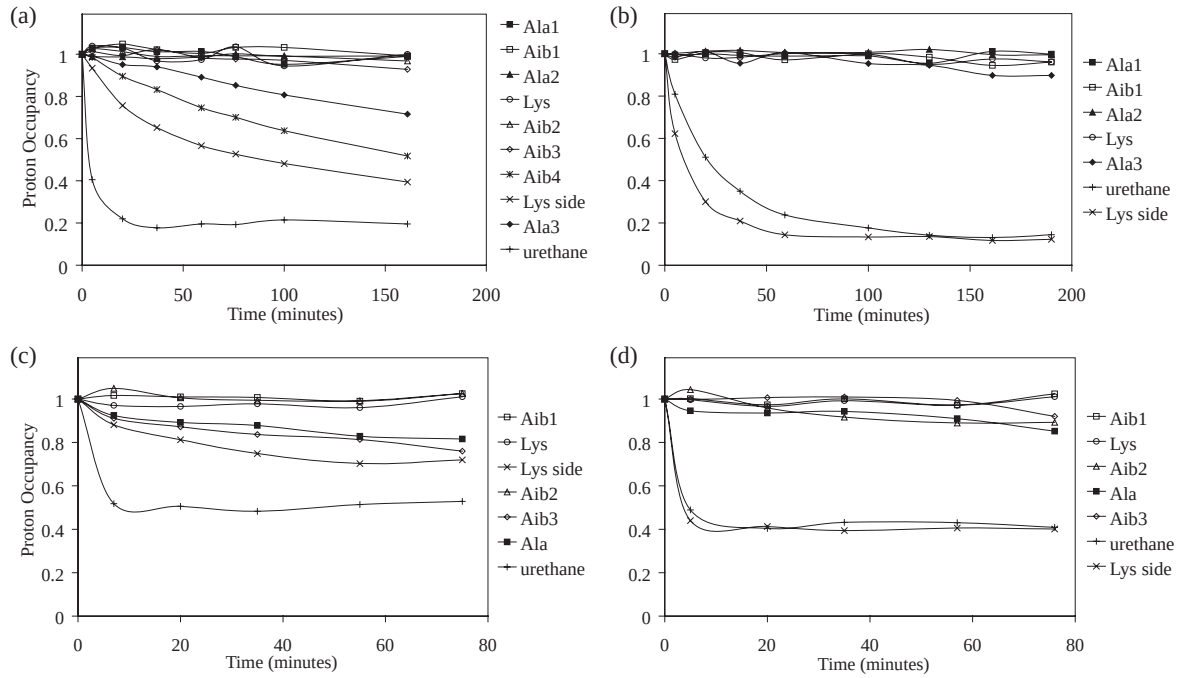

Fig. 7. Deuterium exchange curves for (a) tri9, (b) mono9, (c) tri6, and (d) mono6 as monitored by NMR in CD_3CN at 298 K.

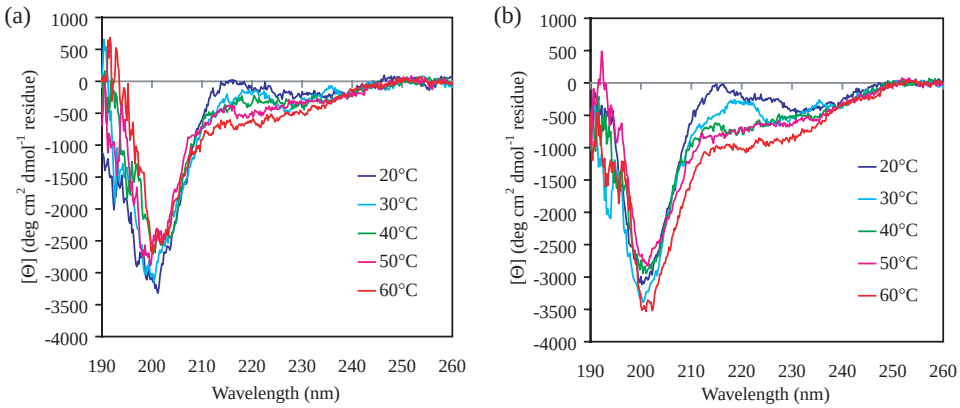

Fig. 8. Temperature-dependence CD spectra of (a) tri6 and (b) mono6 in ethanol.

nal and *C*-terminal of helices on the basis of dipole–dipole interactions. As a result, the urethane and amide protons around the terminals of the helices in tri9 are likely to be exposed to solvent. Similar trends were observed in deuterium exchange rates of tri6 and mono6 (Figs. 7c and 7d). According to the interpretation, deuterium exchange rates of amide protons should be accelerated in the helix-peptide wheels compared to the respective linear helix peptides due to the bending strain on the cylindrical helix by dipole–dipole interaction. Taken together, the predominant structure of the helix-peptide wheels is a planar triangle in solution.

The amide proton of Ala2 in tri9 was shown to be exposed to solvent (Fig. 3b), but its deuterium exchange rate was small (Fig. 7a). The small exchange rate was also observed with amide protons of mono9 (Fig. 7b). It is therefore speculated that the exchange process of amide protons at *N*-terminal should be suppressed, even though they are not involved in hydrogen bonds. A plausible reason is that the positive partial charge of the helix dipole should suppress the protonation of carbonyl oxygen followed by the amide proton release, which is the initial part of the deuterium exchange reaction by the acid catalysis mechanism.[15]

Temperature Dependence of CD. To investigate thermal stability of these peptides in solution, temperature-dependency of CD spectra was studied in ethanol. The spectra of tri6 and mono6 changed similarly with an increase in temperature, and the intensities of the Cotton effects were small (Fig. 8). Therefore, the helices are not so stable in these peptides. In contrast, there was hardly any change observed in spectra for tri9 upon changing the temperature. On the other hand, the reference compound mono9 showed a decrease in intensity around 203 nm at 60 °C (Fig. 9). These results indicate that helices are stabilized significantly in tri9, suggesting that intramolecular dipole–dipole interaction should contribute to the thermal stability of the helices.

Helix-Peptide Wheels on Gold. The monolayer formation of these helix-peptide wheels was studied. The helix-peptide wheels were spread at the air/water interface, and the mono-

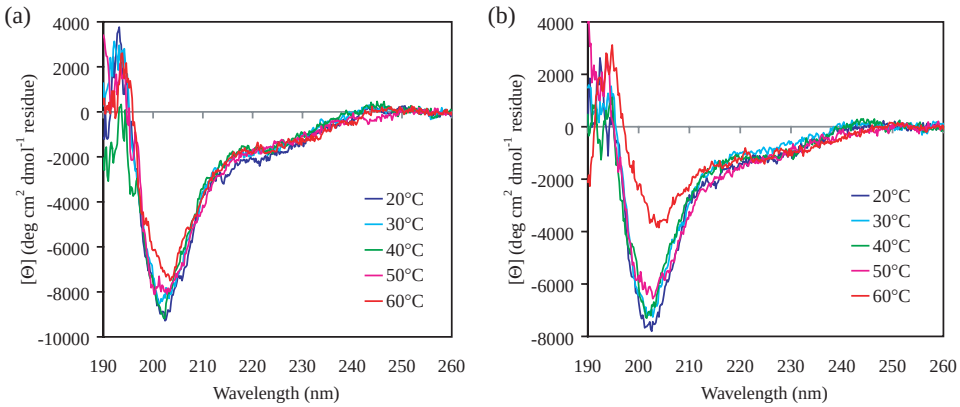

Fig. 9. Temperature-dependence CD spectra of (a) tri9 and (b) mono9 in ethanol.

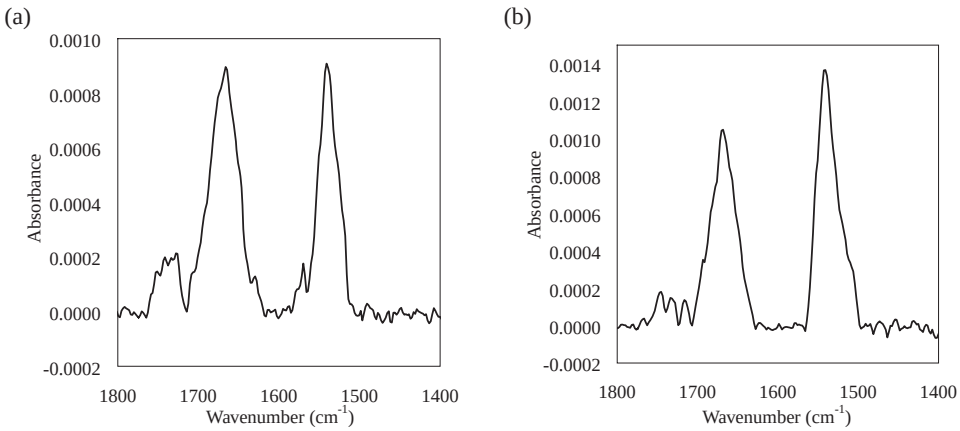

Fig. 10. IRRAS spectra of LB films of (a) tri6 and (b) tri9.

layers were transferred onto gold-coated glass substrates by using a vertical dipping method. The thicknesses of the monolayers were measured by ellipsometry to be 14 and 11 Å for tri6 and tri9, respectively. The calculated thickness either of tri6 or tri9 monolayer was 11 Å under the assumption that they have a coplanar structure with a horizontal orientation on the gold, which is close to the observed values.

Further, the monolayers on gold were subjected to IRRAS to evaluate the molecular orientation on gold. The IRRAS spectra of the monolayers of tri6 and tri9 are shown in Fig. 10. In both spectra, amide I and amide II were observed at around 1665 and 1540 cm^{-1}, respectively. From the amide I/amide II absorbance ratio, the tilt angles of the helix axes of tri6 and tri9 from the surface were calculated to be 65 and 72°, respectively.[8] Therefore, this result also supports a horizontal orientation of the helices on the gold surface.

Taken together, the monolayers of the helix-peptide wheels were successfully prepared on the gold substrate with coplanar structures and a horizontal orientation to gold surface. Although the molecular sizes of the helix-peptide wheels are very large, these monolayers were densely and regularly packed on gold.

Conclusion

Two novel helix-peptide wheels, in which three helices were connected in the middle of these helices by using a template, were prepared. From the results of spectroscopic measurements, the helical segments of the helix-peptide wheels had a 3_{10}-helix structure, and the predominant structure of the helix-peptide wheels was a planar triangle in solution stabilized by intramolecular dipole–dipole interactions between the helical segments. Further, this unique triangle structure was successfully transferred onto a gold substrate. As demonstrated in the present study, intramolecular dipole–dipole interactions among helical peptides are helpful to regulate the molecular shape uniquely. It is expected that the structure of the helix-peptide wheels can be influenced by applying an external stimulus, such as electric field, due to the interactions with the large dipole moments of the helices.[16] The control of the structure of the helix-peptide wheel on substrate by applying electric field is now under investigation.

This work is partly supported by Grant-in-Aids for Young Scientists B (No. 16750098), for Exploratory Research (No. 17655098), and for Scientific Research B (No. 15350068), and 21st century COE program, COE for a United Approach to New Materials Science, from the Ministry of Education, Culture, Sports, Science and Technology, Japan.

References

1 a) J. Zhu, X.-Z. Wang, Y.-Q. Chen, X.-K. Jiang, X.-Z. Chen, Z.-T. Li, *J. Org. Chem.* **2004**, *69*, 6221. b) B. Huang, J. R. Parquette, *J. Am. Chem. Soc.* **2001**, *123*, 2689.

2 M. S. Cubberley, B. L. Iverson, *J. Am. Chem. Soc.* **2001**,

123, 7560.
3 D. J. Hill, J. S. Moore, *Proc. Natl. Acad. Sci. U.S.A.* **2002**, *99*, 5053.
4 K. Yoshida, S. Kawamura, T. Morita, S. Kimura, *J. Am. Chem. Soc.* **2006**, *128*, 8034.
5 C. Baraguey, D. Mertens, A. Dolle, *J. Phys. Chem. B* **2002**, *106*, 6331.
6 *Cache Worksystems Pro Version 6.1.1*, Fujitsu Limited, Tokyo, **2003**.
7 C. Tonlolo, E. Benedetti, *Trends Biochem. Sci.* **1991**, *16*, 350.
8 Y. Miura, S. Kimura, Y. Imanishi, J. Umemura, *Langmuir* **1998**, *14*, 2761.
9 K. Yanagisawa, T. Morita, S. Kimura, *J. Am. Chem. Soc.* **2004**, *126*, 12780.
10 C. Toniolo, A. Polese, F. Formaggio, M. Crisma, J. Kamphuis, *J. Am. Chem. Soc.* **1996**, *118*, 2744.
11 K. Otoda, Y. Kitagawa, S. Kimura, Y. Imanishi, *Biopolymers* **1993**, *33*, 1337.
12 Y. Inai, T. Hirabayashi, *Biopolymers* **2001**, *59*, 356.
13 S. Kimura, Y. Imanishi, *Biopolymers* **1983**, *22*, 2191.
14 C. A. Rohl, R. L. Baldwin, *Biochemistry* **1997**, *36*, 8435.
15 C. A. Rohl, R. L. Baldwin, *Biochemistry* **1994**, *33*, 7760.
16 K. Kitagawa, T. Morita, S. Kimura, *Angew. Chem., Int. Ed.* **2005**, *44*, 6330.